Jet Radius and Momentum Splitting Fraction with Dynamical Grooming in Heavy-Ion Collisions

Lei Wang(王磊)[1], Jin-Wen Kang(康锦文)[1], Qing Zhang(张清)[1], Shuwan Shen(申淑婉)[1], Wei Dai(代巍)[2*], Ben-Wei Zhang(张本威)[1,3*], and Enke Wang(王恩科)[1,3]

[1]*Key Laboratory of Quark and Lepton Physics (MOE) and Institute of Particle Physics, Central China Normal University, Wuhan 430079, China*
[2]*School of Mathematics and Physics, China University of Geosciences (Wuhan), Wuhan 430074, China*
[3]*Guangdong Provincial Key Laboratory of Nuclear Science, Institute of Quantum Matter, South China Normal University, Guangzhou 510006, China*

(Received 14 December 2022; accepted manuscript online 27 February 2023)

We investigate the medium modifications of momentum splitting fraction and groomed jet radius with both dynamical grooming and soft drop algorithms in heavy-ion collisions. In the calculation, the partonic spectrum of initial hard scattering in p+p collisions is provided by the event generator PYTHIA8, and the energy loss of fast parton traversing in a hot/dense quantum-chromodynamic medium is simulated with the linear Boltzmann transport model. We predict the normalized distributions of the groomed jet radius $\theta_{\rm g}$ and momentum splitting fraction $z_{\rm g}$ with the dynamical grooming algorithm in Pb+Pb collisions at $\sqrt{s_{\rm NN}} = 5.02\,\text{TeV}$, then compare these quantities in dynamical grooming at $a = 0.1$, with that in soft drop at $z_{\rm cut} = 0.1$ and $\beta = 0$. It is found that the normalized distribution ratios Pb+Pb/p+p with respect to $z_{\rm g}$ in $z_{\rm cut} = 0.1$, $\beta = 0$ soft drop case are close to unity, those in $a = 0.1$ dynamical grooming case show enhancement at small $z_{\rm g}$, and Pb+Pb/p+p with respect to $\theta_{\rm g}$ in the dynamical grooming case demonstrate weaker modification than those in the soft drop counterparts. We further calculate the groomed jet number averaged momentum splitting fraction $\langle z_{\rm g}\rangle_{\rm jets}$ and averaged groomed jet radius $\langle\theta_{\rm g}\rangle_{\rm jets}$ in p+p and A+A for both grooming cases in three $p_{\rm T}^{\rm ch\ jet}$ intervals, and find that the originally generated well balanced groomed jets will become more momentum imbalanced and jet size less narrowed due to jet quenching, and weaker medium modification of $z_{\rm g}$ and $\theta_{\rm g}$ in the $a = 0.1$ dynamical grooming case than in the soft drop counterparts.

DOI: 10.1088/0256-307X/40/3/032101

In high-energy proton-proton and nucleus-nucleus collisions, a series of new jet substructure observables are measured and analyzed from the experiment at the Large Hadron Collider (LHC). The studies of these jet substructures served as powerful tools to probe the fundamental properties of quantum chromodynamics (QCD) and nucleon structure.[1–4] They also provide new opportunities to probe the properties of the hot dense medium, quark-gluon plasma (QGP) created in heavy-ion collisions.[5–10] The momentum splitting fraction $z_{\rm g}$ and the jet splitting angle $\theta_{\rm g}$ describe the basic properties of the primary splitting structure of a jet are emerged, and they have been measured in heavy-ion collisions both at RHIC and LHC energies.[11,12] Some of them have been tested against parton energy loss models.[13–21]

The research of these jet substructures requires the definition of the jet grooming techniques,[22,23] which is utilized to isolate branches of a jet that corresponds to a hard splitting by removing soft wide-angle radiation. Soft drop grooming algorithm,[24–26] as one of the techniques, is defined by setting a condition $z_{\rm g} > z_{\rm cut}\theta_{\rm g}^{\beta}$ to remove soft wide-angle radiation inside a jet. Thus, the groomed momentum splitting fraction of the two branches $z_{\rm g}$ and the angle of the remaining branches $\theta_{\rm g}$ have been studied in experiment[27,28] and theory.[29–32] Since the soft drop algorithm exhibits the sensitivities to the values of the soft threshold $z_{\rm cut}$ and the angular exponent β, a new method called dynamical grooming[33–35] was proposed to suppress these sensitivities. It is more closely aligned with the intrinsic properties of a given jet and does not require fine-tuning. The grooming condition in dynamical grooming defines a maximum rather than an explicit cut as in soft drop, thus, every dynamically groomed jet will always return a splitting. However, it is possible that a jet does not contain any splitting even after it satisfies the grooming condition in soft drop. It is important to directly compare the jet substructure observables for inclusive jets with two jet grooming algorithms in p+p collisions. ALICE experiments[36] measured the normalized momentum splitting fraction $z_{\rm g}$ and groomed jet radius $\theta_{\rm g}$ with the dynamical grooming and the soft drop grooming algorithms in proton-proton collisions at $\sqrt{s} = 5.02\,\text{TeV}$ in $60 < p_{\rm T,jet} < 80\,\text{GeV}/c$, respectively. It is meaningful to calculate these two observables in Pb+Pb collisions in both

*Corresponding authors. Email: weidai@cug.edu.cn; bwzhang@mail.ccnu.edu.cn
© 2023 Chinese Physical Society and IOP Publishing Ltd

grooming algorithms, since the soft drop case is already in place,[25] the prediction in the dynamical grooming case is urgently needed. Furthermore, the ALICE reports the first measurement of these two jet substructure observables in the $a = 0.1$ dynamical grooming case and the $z_{\rm cut} = 0.1$, $\beta = 0$ soft drop grooming case. It would also be interesting to directly compare the medium modification of the groomed jet substructure observables in these two jet grooming cases.

In this Letter, firstly we introduce the framework used to calculate the normalized groomed jet radius and momentum splitting fraction with the soft drop and dynamical grooming algorithms in p+p and Pb+Pb collisions. Secondly, we present predictions for the distributions of $z_{\rm g}$ and $\theta_{\rm g}$ in central 0–30% Pb+Pb collisions at $\sqrt{s_{\rm NN}} = 5.02\,\text{TeV}$ for inclusive jets with dynamical grooming using different dynamical grooming parameter $a = 0.1$, 1, 2. Then, We compare the medium modification of jet substructures for the groomed jets selected from the $a = 0.1$ case in the dynamical grooming and from the $z_{\rm cut} = 0.1, \beta = 0$ case in soft drop. In the end, we systematically investigate the jet substructure observables $z_{\rm g}$ and $\theta_{\rm g}$ for inclusive jets in p+p and Pb+Pb collisions at $\sqrt{s} = 5.02\,\text{TeV}$ in both the $z_{\rm cut} = 0.1$, $\beta = 0$ soft drop grooming case and the $a = 0.1$ dynamical grooming case.

Analysis Framework. We start with the impact of the dynamical grooming algorithm and the soft drop grooming algorithm to the jet substructure observables $z_{\rm g}$ and $\theta_{\rm g}$ of inclusive jets in p+p collisions at $\sqrt{s} = 5.02\,\text{TeV}$. The dynamical grooming algorithm[33] identifies a single splitting in the primary Lund plane[37] that maximizes

$$z_i(1 - z_i)p_{{\rm T},i}\,\theta_i^a, \tag{1}$$

over all splittings in the plane, with

$$z_i = \frac{p_{\rm T}^{{\rm sub},i}}{p_{\rm T}^{{\rm leading},i} + p_{\rm T}^{{\rm sub},i}},$$
$$\theta_i = \Delta R_i/R. \tag{2}$$

Here $p_{\rm T}^{{\rm leading},i}$ and $p_{\rm T}^{{\rm sub},i}$ are the transverse momenta of the leading jet and subleading jet, respectively. $\Delta R_i = \sqrt{\Delta y_i^2 + \Delta\phi_i^2}$ is the rapidity-azimuth separation of the splitting, and the exponent a is a free parameter that defines the density of the phase space in the Lund plane that is groomed away. For different parameter a, it has different physical significance, the parameter $a = 0$ in the dynamical grooming algorithm corresponds to the case we select the splitting with the most symmetric momentum sharing according to Eq. (1); $a = 1$ refers to the case we prefer the branching with the largest transverse momentum; $a = 2$ means we select the splitting with the shortest formation time.[33,34] Since $a = 0$ is formally collinear unsafe,[33] we use $a = 0.1$ instead in this investigation. On the other hand, the soft drop grooming algorithm implements much simpler grooming conditions, $z_i > z_{\rm cut}\theta_i^\beta$. It is designed to remove soft wide-angle radiation from a jet. The parameter $\beta = 0$ in the soft drop grooming algorithm indicates that it will groom away splittings below a certain $z_{\rm cut}$.

We computed in Fig. 1 the normalized momentum splitting fraction $z_{\rm g}$ and groomed jet radius $\theta_{\rm g}$ with the dynamical grooming (left panels) and the soft drop grooming (right panels) algorithms in proton-proton collisions at $\sqrt{s} = 5.02\,\text{TeV}$ in $60 < p_{\rm T,jet} < 80\,\text{GeV}/c$. A Monte Carlo model PYTHIA8[38] is used to generate charged jets. They are reconstructed by the anti-$k_{\rm T}$ algorithm[39] with the jet radius $R = 0.4$ and selected according to the same kinematic cuts as adopted by the experimental measurements.[36]

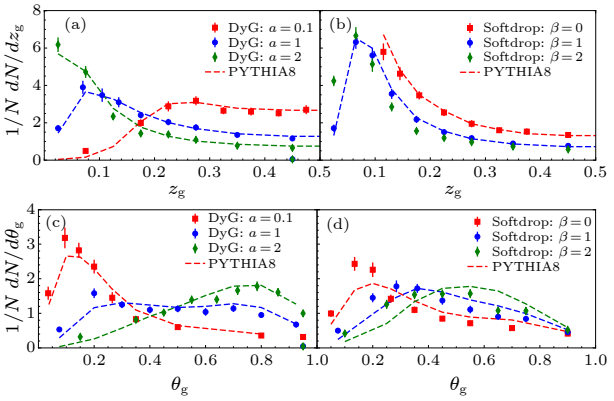

Fig. 1. Normalized $z_{\rm g}$ and $\theta_{\rm g}$ distributions for inclusive jets with the soft drop and the dynamical grooming algorithms in p+p collisions at $\sqrt{s} = 5.02\,\text{TeV}$ from PYTHIA8 calculation in comparison with the ALICE data.[36]

Our calculation results are consistent with the experimental data in p+p collisions at $\sqrt{s} = 5.02\,\text{TeV}$ in both the dynamical grooming case and the soft drop grooming case. In the soft drop grooming case, the $z_{\rm g}$ values with $\beta = 0$, 1, 2 are all tend to distribute in the smaller $z_{\rm g}$, $\beta = 0$ case is the most balanced preference among those of $\beta = 0$, 1, 2. Interestingly, despite of the fact that $a = 1$, 2 in the dynamical grooming case also tend to the distributed in the smaller $z_{\rm g}$, the $a = 0.1$ case in the dynamical grooming selects the most balanced jets in which the groomed jet samples are much more distributed at larger $z_{\rm g}$ value. In the right bottom panel in Fig. 1, we find that, in the $\beta = 0$ case, which corresponds to the most symmetric momentum sharing in the soft drop grooming, the jet sample tends to distribute in the smallest $\theta_{\rm g}$ region. The larger the β is, the broader the groomed jet samples are. In the left bottom panel, the most balanced jets selected by dynamical grooming with the parameter $a = 0.1$ will be much more concentrated at the smaller $\theta_{\rm g}$. As the parameter a increases, the radius of the groomed jets tends to be much larger. Such sensitivity due to the variation of the groomed parameter is much more dramatic than the soft drop case. It is noticed that the case $a = 0.1$ selects the splitting with largest z, and is similar to the $\beta = 0$ case in the soft drop, which grooms away splittings below a certain z, but the $a = 0.1$ case in dynamical grooming selects much more balanced groomed jets. It would be interesting to directly compare the medium modification of the groomed jets substructure in these two cases.

The medium modification of jets is simulated within

the linear Boltzmann transport (LBT) model[13,40–42] that includes both elastic and inelastic processes of parton scattering for jet shower and thermal recoil partons in the QGP medium. The elastic scattering is described by the linear Boltzmann equation:

$$\begin{aligned} & p_1 \cdot \partial f_a(p_1) \\ = & -\int \frac{d^3p_2}{(2\pi)^3 2E_2} \int \frac{d^3p_3}{(2\pi)^3 2E_3} \int \frac{d^3p_4}{(2\pi)^3 2E_4} \\ & \times \frac{1}{2} \sum_{b(c,d)} [f_a(p_1) f_b(p_2) - f_c(p_3) f_d(p_4)] |M_{ab\to cd}|^2 \\ & \times S_2(s,t,u)(2\pi)^4 \delta^4(p_1 + p_2 - p_3 - p_4), \end{aligned} \tag{3}$$

where f_i $(i = a, b, c, d)$ are the phase-space distributions of medium parton, $S_2(s,t,u) = \theta(s \geq 2\mu_{\rm D}^2)\theta(-s + \mu_{\rm D}^2 \leq t \leq -\mu_{\rm D}^2)$ is a Lorentz invariant condition to regulate the collinear $(t, u \to 0)$ divergence of the matrix element $|M_{ab\to cd}|^2$, with $\mu_{\rm D}^2 = g^2T^2(N_c + N_f/2)/3$ being the Debye screening mass. The inelastic scattering is described by the higher twist formalism for induced gluon radiation.[16,43–45] The evolution of bulk medium is given by the 3+1D CLVisc hydrodynamical model[46,47] under initial conditions simulated from a multi-phase transport (AMPT) model.[48,49] Parameters used in the CLVisc are fixed by reproducing hadron spectra with experimental measurements. The LBT model has been used to provide a nice description of a series of jet quenching measurements, such as bosons tagged jet/hadron production,[50,51] light and heavy flavor hadrons suppression, and single inclusive jets suppression.[40,41] After the in-medium evolution, the hadronization of partons is performed by the hadronization method of JETSCAPE,[52] which was based on the Lund string model[53] provided by PYTHIA8.

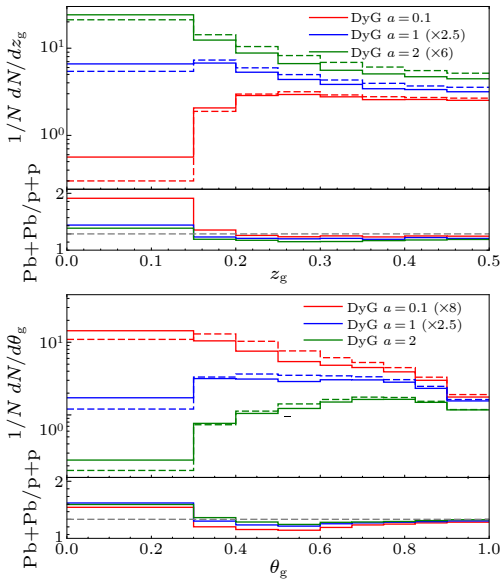

Fig. 2. Normalized $z_{\rm g}$ and $\theta_{\rm g}$ distributions in p+p and $0-30\%$ Pb+Pb collisions at $\sqrt{s} = 5.02\,\text{TeV}$ in $p_{\rm T,jet}$ interval $60 < p_{\rm T,jet} < 80\,\text{GeV}/c$ for inclusive jets with the dynamical grooming algorithm for some values of grooming parameter $a = 0.1$, 1, 2. The dashed line is for p+p collisions and the solid line is for Pb+Pb collisions.

Numerical Results and Discussions. We firstly predict in Fig. 2, the $z_{\rm g}$ and $\theta_{\rm g}$ distributions in central 0–30% Pb+Pb collisions at $\sqrt{s_{\rm NN}} = 5.02\,\text{TeV}$ for inclusive jets with dynamical grooming algorithms using different dynamical grooming parameters $a = 0.1$, 1, 2. In order to focus on the jet quenching effect, the jet radius parameter $R = 0.2$ is selected. In the three cases of groomed parameters a, the normalized $z_{\rm g}$ and $\theta_{\rm g}$ distributions in Pb+Pb collisions will shift to smaller value compared to that in p+p collisions, leading to enhancement in smaller $z_{\rm g}$ ($\theta_{\rm g}$) and suppression in larger $z_{\rm g}$ ($\theta_{\rm g}$) as demonstrated in the upper panels. In order to distinguish the distributions for better presentation, different factors have been multiplied to different curves. To better understand the detail of the medium modification, the ratios of the normalized distributions in Pb+Pb and p+p are plotted in the bottom panels. We find that, with the decreasing parameter a, more proportion of the groomed jets in A+A is observed to shift towards smaller $z_{\rm g}$ compared to that in p+p, and less proportion of the groomed jets in A+A is observed to shift towards smaller $\theta_{\rm g}$. This indicates that, in the context of dynamical grooming algorithm, the originally triggered more balanced dynamical groomed jets will become more momentum imbalanced and less narrow due to jet quenching.

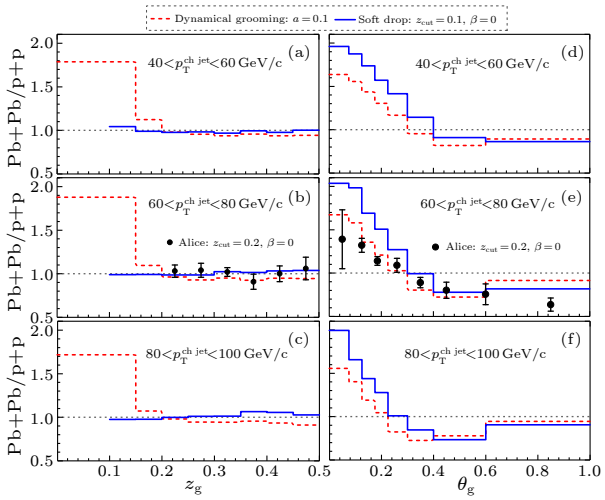

Fig. 3. The Pb+Pb/p+p ratios of normalized $z_{\rm g}$ (upper plots) and $\theta_{\rm g}$ (bottom plots) distribution with the soft drop and the dynamical grooming algorithms at $\sqrt{s} = 5.02\,\text{TeV}$ in different $p_{\rm T,jet}$ intervals $40 < p_{\rm T,jet} < 60\,\text{GeV}/c$, $60 < p_{\rm T,jet} < 80\,\text{GeV}/c$, and $80 < p_{\rm T,jet} < 100\,\text{GeV}/c$ from top to bottom, respectively.

Next, we compare the medium modification of jet substructures for the groomed jets selected from the $a = 0.1$ case in the dynamical grooming algorithm and from the $z_{\rm cut} = 0.1, \beta = 0$ case in the soft drop grooming algorithm scenario. The two cases that we selected to compare can both help to generate the most momentum balanced groomed jets in their own categories, and the groomed jets generated from the $a = 0.1$ case in the dynamical grooming algorithm are much more balanced, as demonstrated in Fig. 1. In Fig. 3, we plot Pb+Pb/p+p ratios

of the normalized distributions as functions of z_g (upper panels) and θ_g (lower panels) in both the grooming cases of inclusive jets in central 0–30% Pb+Pb collisions at $\sqrt{s_{NN}} = 5.02$ TeV, for three different jet transverse momentum intervals: $40 < p_T^{\text{ch jet}} < 60$ GeV/c, $60 < p_T^{\text{ch jet}} < 80$ GeV/c and $80 < p_T^{\text{ch jet}} < 100$ GeV/c, respectively, from left to right panels. In all three different jet transverse momentum intervals, the Pb+Pb/p+p ratios of the normalized z_g distributions within $z_{cut} = 0.1$, $\beta = 0$ in the soft drop grooming algorithm are close to unity, the observations are in consistent with the experimental measurements.[25] However, within $a = 0.1$ in the dynamical grooming case, the Pb+Pb/p+p ratios of the normalized z_g distributions show enhancement in smaller z_g and suppression in larger z_g, as demonstrated in the upper plots. It implies that those most balanced jets, which are groomed by the dynamical grooming algorithm in p+p, are much more modified due to jet quenching compared to that of the soft drop counterparts, leading to stronger normalized distribution shifting towards small z_g. However, the Pb+Pb/p+p ratio comparisons of the two cases with respect to θ_g in lower plots show that the most balanced jets in p+p would suffer weaker normalized distribution shifting towards small θ_g due to the medium modification compared to that of the soft drop counterparts. The increase of jet transverse momentum will lead to the stronger distribution shifting of θ_g towards smaller values. The ALICE experimental data for the $z_{cut} = 0.2$, $\beta = 0$ case is also plotted accordingly for reference. To conclude the above observation, the jet quenching effect will lead to the groomed jets in both the cases to become momentum imbalance and size narrower, the originally generated more momentum balanced groomed jets in p+p would become more momentum imbalance and less narrow.

Table 1. The averaged momentum splitting fraction in inclusive jets with the soft drop grooming and the dynamical grooming algorithms, calculated in both p+p and Pb+Pb collisions at $\sqrt{s} = 5.02$ TeV at three transverse momentum intervals: $40 < p_T^{\text{ch jet}} < 60$ GeV/c, $60 < p_T^{\text{ch jet}} < 80$ GeV/c and $80 < p_T^{\text{ch jet}} < 100$ GeV/c, respectively.

$P_T^{\text{ch jet}}$	Soft drop: $z_{cut} = 0.1$, $\beta = 0$	Dynamical grooming: $a = 0.1$	
	$\langle z_g \rangle_{\text{jets}}$	$\langle z_g \rangle_{\text{jets}}$	
40–60 GeV	0.232	0.322	p+p
	0.210	0.312	A+A
60–80 GeV	0.224	0.319	p+p
	0.200	0.308	A+A
80–100 GeV	0.217	0.317	p+p
	0.196	0.304	A+A

Furthermore, we systematically investigate the jet substructure observables z_g and θ_g for inclusive jets in p+p and Pb+Pb collisions at $\sqrt{s} = 5.02$ TeV in both the $z_{cut} = 0.1$, $\beta = 0$ soft drop grooming case and the $a = 0.1$ dynamical grooming case. We list the number of groomed jets averaged momentum sharing of the groomed inclusive jets in p+p and A+A in both the two cases for all three jet p_T intervals in Table 1 and the results of the number of groomed jets averaged groomed jet radius in Table 2. We find that, in p+p, the averaged splitting fraction $\langle z_g \rangle_{\text{jets}}$ (the averaged groomed jet radius $\langle \theta_g \rangle_{\text{jets}}$) in the $a = 0.1$ dynamical grooming case is always larger (smaller) than that in the $z_{cut} = 0.1$, $\beta = 0$ soft drop grooming case in all $p_T^{\text{ch jet}}$ intervals, and the higher the $p_T^{\text{ch jet}}$ is, the smaller the value of the $\langle z_g \rangle_{\text{jets}}$ and the $\langle \theta_g \rangle_{\text{jets}}$ are. It means that the $a = 0.1$ dynamical grooming case always tends to generate more momentum balanced and narrower groomed jets in all $p_T^{\text{ch jet}}$ intervals than the $z_{cut} = 0.1$, $\beta = 0$ soft drop grooming case, and higher $p_T^{\text{ch jet}}$ always tends to generate more momentum imbalanced and narrower sized groomed jets in both the cases.

Table 2. The averaged groomed jet radius in inclusive jets with the soft drop grooming and the dynamical grooming algorithms, calculated in both p+p and Pb+Pb collisions at $\sqrt{s} = 5.02$ TeV at three transverse momentum intervals: $40 < p_T^{\text{ch jet}} < 60$ GeV/c, $60 < p_T^{\text{ch jet}} < 80$ GeV/c and $80 < p_T^{\text{ch jet}} < 100$ GeV/c, respectively.

$P_T^{\text{ch jet}}$	Soft drop: $z_{cut} = 0.1$, $\beta = 0$	Dynamical grooming: $a = 0.1$	
	$\langle \theta_g \rangle_{\text{jets}}$	$\langle \theta_g \rangle_{\text{jets}}$	
40–60 GeV	0.582	0.478	p+p
	0.539	0.443	A+A
60–80 GeV	0.497	0.397	p+p
	0.441	0.358	A+A
80–100 GeV	0.424	0.333	p+p
	0.383	0.310	A+A

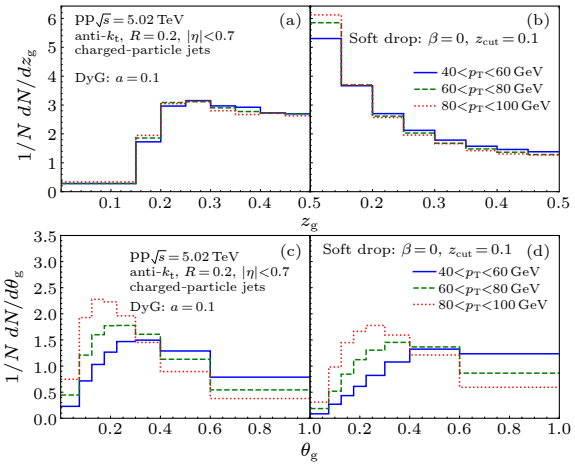

Fig. 4. Normalized z_g and θ_g distributions for inclusive jets with the soft drop and the dynamical grooming algorithms in p+p collisions at $\sqrt{s} = 5.02$ TeV from PYTHIA8 calculation in different p_T intervals.

The values of the $\langle z_g \rangle_{\text{jets}}$ and $\langle \theta_g \rangle_{\text{jets}}$ in A+A are consistently smaller than those in p+p for both the grooming cases in all three $p_T^{\text{ch jet}}$ intervals. It indicates that, despite of the different grooming methods, the originally generated more balanced groomed jets will become more momentum imbalanced and jet size less narrowed due to jet quenching. We find $\langle z_g \rangle_{\text{jets}}^{\text{pp}} - \langle z_g \rangle_{\text{jets}}^{\text{AA}} \approx 0.01$ for the $a = 0.1$ dynamical grooming case, and ≈ 0.02 for the $z_{cut} = 0.1$, $\beta = 0$ soft drop grooming case in all the three $p_T^{\text{ch jet}}$ in-

tervals, indicating overall weaker medium modification of z_g for those originally more balanced groomed jets generated in the $a = 0.1$ dynamical grooming case than that in the soft drop case. We conduct the same comparison to $\langle\theta_g\rangle_{jets}^{pp} - \langle\theta_g\rangle_{jets}^{AA}$ for both the cases, find the same overall weaker medium modification of θ_g for those originally more balanced and narrower groomed jets generated in the $a = 0.1$ dynamical grooming case than that in the soft drop case.

Naively, we expect that the soft gluon radiation processes in jet quenching will induce the energy in a jet to distribute at larger radius and the energies of the primary two splitting sub-jets to be more imbalanced. Throughout the investigation, we find that the A+A groomed jets always become momentum imbalanced and narrower compared to the p+p counterparts due to quenching for all grooming cases in all the three $p_T^{ch\ jet}$ intervals. Due to the fact that the p_T interval we compared in Pb+Pb collisions is the same as that in p+p collisions, they can be the groomed jets with originally higher $p_T^{ch\ jet}$ in p+p that distributed at smaller z_g and θ_g to fall into the $p_T^{ch\ jet}$ intervals we investigated. As we can see in Fig. 4, when the $p_{T,jet}$ intervals increase, the distributions of z_g and θ_g in p+p collisions move towards smaller values, which indicate momentum imbalance and narrower splitting, respectively. Therefore, one sees why the z_g and θ_g become smaller in A+A compared to that in p+p.

In summary, we have systematically predicted the normalized distributions of the groomed jet radius θ_g and momentum splitting fraction z_g with the dynamical grooming algorithms in Pb+Pb collisions at $\sqrt{s_{NN}} = 5.02$ TeV. It is found that in the context of dynamical grooming algorithm, more balanced dynamical groomed jets generated by smaller parameter a in p+p will become more momentum imbalanced and less jet size due to jet quenching. By comparing these jet substructure observables with different parameters in these two grooming cases in p+p, we find that the $a = 0.1$ dynamical grooming case would generate the most momentum balanced groomed jets, thus a systematical comparison with the most balanced case in the soft drop grooming $z_{cut} = 0.1$, $\beta = 0$ is conducted. The normalized distribution ratios Pb+Pb/p+p with respect to z_g in the $z_{cut} = 0.1$, $\beta = 0$ soft drop case are close to unity and those in the $a = 0.1$ dynamical grooming case shows enhancement at small z_g. Pb+Pb/p+p with respect to θ_g in the dynamical grooming case demonstrates weaker modification than those in the soft drop counterparts. We further calculate the groomed jet number averaged momentum splitting fraction $\langle z_g\rangle_{jets}$ and averaged groomed jet radius $\langle\theta_g\rangle_{jets}$ in p+p and A+A for both the grooming cases in all the three $p_T^{ch,jet}$ intervals. We find that the originally generated more balanced groomed jets will become more momentum imbalanced and jet size less narrowed due to jet quenching, and weaker medium modification of z_g and θ_g in the $a = 0.1$ dynamical grooming case than that in the soft drop counterpart.

Acknowledgments. This work was supported by the Guangdong Major Project of Basic and Applied Basic Research (Grant No. 2020B0301030008), the Natural Science Foundation of China (Grant Nos. 11935007 and 11805167).

References

[1] Sterman G F and Weinberg S 1977 *Phys. Rev. Lett.* **39** 1436
[2] Altheimer A, Arora S, Asquith L *et al.* 2012 *J. Phys. G* **39** 063001
[3] Altheimer A, Arce A, Asquith L *et al.* 2014 *Eur. Phys. J. C* **74** 2792
[4] Marzani S, Soyez G, and Spannowsky M 2019 *Looking inside jets: an introduction to jet substructure and boosted-object phenomenology* (Springer)
[5] Acharya S, Adamová D, Adler A *et al.* (ALICE collaboration) 2022 *J. High Energy Phys.* 2022(05) 061
[6] Casalderrey-Solana J, Milhano G, Pablos D, and Rajagopal K 2020 *J. High Energy Phys.* 2020(01) 044
[7] Vitev I and Zhang B W 2010 *Phys. Rev. Lett.* **104** 132001
[8] Vitev I, Wicks S, and Zhang B W 2008 *J. High Energy Phys.* 2008(11) 093
[9] Andrews H A, Apolinario L, Bertens R A *et al.* 2020 *J. Phys. G* **47** 065102
[10] Acharya S, Adamová D, Adhya S P *et al.* (ALICE collaboration) 2020 *Phys. Lett. B* **802** 135227
[11] Abdallah M S, Aboona B E, Adam J *et al.* (STAR collaboration) 2022 *Phys. Rev. C* **105** 044906
[12] Aaboud M, Abbott B, Abdinov O *et al.* (ATLAS collaboration) 2019 *Phys. Rev. Lett.* **123** 042001
[13] Wang X N and Zhu Y 2013 *Phys. Rev. Lett.* **111** 062301
[14] Majumder A 2013 *Phys. Rev. C* **88** 014909
[15] Zapp K, Ingelman G, Rathsman J, Stachel J, and Wiedemann U A 2009 *Eur. Phys. J. C* **60** 617
[16] Zhang B W, Wang E, and Wang X N 2004 *Phys. Rev. Lett.* **93** 072301
[17] Dai W, Wang S, Zhang S L, Zhang B W, and Wang E 2020 *Chin. Phys. C* **44** 104105
[18] Dai W, Li M Z, Zhang B W, and Wang E 2022 arXiv:2205.14668 [hep-ph]
[19] Wang S, Dai W, Zhang B W, and Wang E 2019 *Eur. Phys. J. C* **79** 789
[20] Schenke B, Gale C, and Jeon S 2009 *Phys. Rev. C* **80** 054913
[21] Armesto N, Cunqueiro L, and Salgado C A 2009 *Eur. Phys. J. C* **63** 679
[22] Dasgupta M, Fregoso A, Marzani S, and Powling A 2013 *Eur. Phys. J. C* **73** 2623
[23] Dasgupta M, Fregoso A, Marzani S, and Salam G P 2013 *J. High Energy Phys.* 2013(09) 029
[24] Larkoski A J, Marzani S, Soyez G, and Thaler J 2014 *J. High Energy Phys.* 2014(05) 146
[25] Acharya S, Adamová D, Adler A *et al.* (A Large Ion Collider Experiment, ALICE collaboration) 2022 *Phys. Rev. Lett.* **128** 102001
[26] Tripathee A, Xue W, Larkoski A, Marzani S, and Thaler J 2017 *Phys. Rev. D* **96** 074003
[27] CMS collaboration 2016 *Splitting Function Pp PbPb Collisions at 5.02 TeV*. Report No. CMS-PAS-HIN-16-006
[28] Kauder K (STAR collaboration) 2017 *Nucl. Part. Phys. Proc.* **289** 137
[29] Chang N B, Cao S, and Qin G Y 2018 *Phys. Lett. B* **781** 423
[30] Chien Y T and Vitev I 2017 *Phys. Rev. Lett.* **119** 112301
[31] Kang Z B, Lee K, Liu X, Neill D, and Ringer F 2020 *J. High Energy Phys.* 2020(02) 054

[32] Ringer F, Xiao B W, and Yuan F 2020 *Phys. Lett. B* **808** 135634

[33] Mehtar-Tani Y, Soto-Ontoso A, and Tywoniuk K 2020 *Phys. Rev. D* **101** 034004

[34] Caucal P, Soto-Ontoso A, and Takacs A 2022 *Phys. Rev. D* **105** 114046

[35] Caucal P, Soto-Ontoso A, and Takacs A 2021 *J. High Energy Phys.* 2021(07) 020

[36] ALICE collaboration 2022 arXiv:2204.10246 [nucl-ex]

[37] Dreyer F A, Salam G P, and Soyez G 2018 *J. High Energy Phys.* 2018(12) 064

[38] Sjöstrand T, Ask S, Christiansen J R, Corke R, Desai N, Ilten P, Mrenna S, Prestel S, Rasmussen C O, and Skands P Z 2015 *Comput. Phys. Commun.* **191** 159

[39] Cacciari M, Salam G P, and Soyez G 2008 *J. High Energy Phys.* 2008(04) 063

[40] He Y Y, Luo T, Wang X N, and Zhu Y 2015 *Phys. Rev. C* **91** 054908

[41] Cao S S, Luo T, Qin G Y, and Wang X N 2016 *Phys. Rev. C* **94** 014909

[42] Cao S S, Luo T, Qin G Y, and Wang X N 2018 *Phys. Lett. B* **777** 255

[43] Guo X F and Wang X N 2000 *Phys. Rev. Lett.* **85** 3591

[44] Zhang B W and Wang X N 2003 *Nucl. Phys. A* **720** 429

[45] Zhang B W, Wang E K, and Wang X N 2005 *Nucl. Phys. A* **757** 493

[46] Pang L G, Wang Q, and Wang X N 2012 *Phys. Rev. C* **86** 024911

[47] Pang L G, Hatta Y, Wang X N, and Xiao B W 2015 *Phys. Rev. D* **91** 074027

[48] Lin Z W, Ko C M, Li B A, Zhang B, and Pal S 2005 *Phys. Rev. C* **72** 064901

[49] Lin Z W and Zheng L 2021 *Nucl. Sci. Tech.* **32** 113

[50] Luo T, Cao S, He Y, and Wang X N 2018 *Phys. Lett. B* **782** 707

[51] Zhang S L, Wang X N, and Zhang B W 2022 *Phys. Rev. C* **105** 054902

[52] Putschke J H, Kauder K, Khalaj E *et al.* 2019 arXiv:1903.07706 [nucl-th]

[53] Sjostrand T 1986 *Comput. Phys. Commun.* **39** 347